JGR Earth Surface

RESEARCH ARTICLE
10.1029/2021JF006509

# Effects of Mass Wasting on the Physiochemical Properties of Fluvial Sediments in Puerto Rico Following Hurricane Maria

**N. D. S. Webb[1], N. R. Regmi[2], G. S. Soreghan[1], A. S. Elwood Madden[1], J. Sylvester[1], F. Cartagena Colon[3], C. Demirel-Floyd[1], and M. E. Elwood Madden[1]**

[1]School of Geosciences, The University of Oklahoma, Norman, OK, USA, [2]Oklahoma Geological Survey, The University of Oklahoma, Norman, OK, USA, [3]University of Puerto Rico at Mayagüez, Mayagüez, Puerto Rico

**Key Points:**

- Hurricane Maria caused shallow landslides that delivered highly weathered soil to streams
- Chemical weathering values were higher in post-hurricane sediments compared to sediments collected before the hurricane
- Shallow landslides due to hurricanes can expose fresh sediment to chemical weathering, thus sequestering carbon via carbonate precipitation

**Supporting Information:**

Supporting Information may be found in the online version of this article.

**Correspondence to:**

N. D. S. Webb,
ninad3612@gmail.com

**Citation:**

Webb, N. D. S., Regmi, N. R., Soreghan, G. S., Elwood Madden, A. S., Sylvester, J., Cartagena Colon, F., et al. (2022). Effects of mass wasting on the physiochemical properties of fluvial sediments in Puerto Rico following Hurricane Maria. *Journal of Geophysical Research: Earth Surface*, *127*, e2021JF006509. https://doi.org/10.1029/2021JF006509

Received 3 NOV 2021
Accepted 12 MAY 2022

**Author Contributions:**

**Conceptualization:** N. D. S. Webb
**Formal analysis:** N. D. S. Webb
**Investigation:** N. D. S. Webb
**Methodology:** N. D. S. Webb
**Writing – original draft:** N. D. S. Webb
**Writing – review & editing:** N. D. S. Webb



**Abstract** Mass wasting plays an important role in carbon cycling and sequestration by exposing fresh bedrock and delivering hillslope sediments to lowlands and fluvial systems. Chemical weathering signatures of landslide-derived fluvial sediments can be used to understand linkages between hillslope and fluvial processes and thus to characterize spatiotemporal dynamics of sediments. However, chemical signatures of fluvial sediments derived by landslides are yet to be fully understood. Here, we compare the bulk chemistry, mineralogy, and grain size of fluvial sediments collected pre- and post-Hurricane Maria in the Rio Guayanés and Rio Guayabo watersheds in southeastern Puerto Rico to help fill this knowledge gap. Comparison of the mud fraction (<63 μm) of fluvial sediments collected before Hurricane Maria with similar mud fractions collected after the storm reveals that the post-hurricane muds exhibit a wider range and higher average weathering index values, but coarser grain size modes. We infer that small landslides triggered by Hurricane Maria transported slope materials from shallow depths, including weathered topsoil and saprolite, as opposed to previous deep-seated landslides, which likely sampled regolith and bedrock. Variances in weathering indices observed that pre- and post-hurricanes do not necessarily reflect average climate signatures, but rather reflect subtle differences in a transport mechanism, which produce significant differences in weathering indices recorded by fluvial sediments. We propose that weathering indices provide a means to understand sediment dynamics in mountainous regions, particularly for sediment transported immediately after landslides triggered by extreme events, such as precipitation and earthquakes, and also provide important data sets required for mapping potential carbon sequestration across landscapes.

**Plain Language Summary** Hurricane Maria caused heavy precipitation and widespread damage across Puerto Rico, including numerous landslides. We mapped the location and size of landslides that occurred in the 6 months following Hurricane Maria and compared sediments collected in June 2018 to samples collected in June 2014 to determine how hurricane-induced landslides affect stream sediments. We found that numerous shallow landslides occurred immediately after Hurricane Maria. Sediments in the stream were more highly weathered than those collected before the hurricane, suggesting that the landslides delivered highly weathered soils to the stream system. This significant change in chemical weathering indices over less than a decade is not indicative of a significant shift in climate, instead the change is likely due to subtle changes in how sediments are delivered to streams via landslides. In addition, changes in stream chemistry post-hurricane suggest that small landslides may lead to significant carbon sequestration as cations released via silicate weathering precipitate carbonate minerals downstream.

## 1. Introduction

Physiochemical characteristics of fluvial sediments have the potential to inform complex linkages among climatic, tectonic, hillslope, and geomorphic processes. For example, weathering trends in fluvial sediments can shed light on rates and frequency of sediment production and transport from upland hillslopes and thus provide a potential signature of both short- and long-term sediment transport and carbon cycling as well as paleoclimate (White et al., 1998, 1999). Mass wasting is one of the major processes that delivers hillslope materials to fluvial systems in moderate- to high-relief settings. Increased mass wasting owing to climate and land-use changes may increase chemical weathering rates (Moore et al., 2019; Oliva et al., 2003), resulting in the consumption of atmospheric carbon dioxide and producing a negative feedback effect for global climate change over thousands to millions of years as well as immediately affecting stream quality and ecology (Sassa & Canuti, 2009).

Chemical weathering of fresh bedrock delivers cations into fluvial systems and draws down $pCO_2$ from the Earth's atmosphere (Berner, 1995; Fernandes et al., 2016). However, landslides may be a net source of $CO_2$ to the atmosphere where the exposure of carbonates and sulfides results in sulfuric acid weathering of the carbonates (Emberson et al., 2018). Thus, the mineralogy of the weathering bedrock plays an important role in determining whether carbon is sequestered or released to the atmosphere. Additionally, landslides can be a potential source of biogenic carbon, and while initial damage to hillside vegetation may be a source of $CO_2$, the subsequent debris can be buried and thus a $CO_2$ sink (Frith et al., 2018).

The relative size and frequency of the landslides also play an important role in determining sediment volume as well as the degree of weathering delivered to the fluvial system. For example, shallow landslides occur frequently and transport highly weathered soil and/or saprolite, whereas deep-seated landslides tend to occur less frequently, but transport large volumes of slope materials, including soil, less-weathered saprolite, and deeper bedrock (Bessette-Kirton et al., 2019; Stark & Hovius, 2001). Landslide size and frequency across a landscape are governed primarily by the spatial structure of hillslope strength variability (Bessette-Kirton et al., 2019; Varnes, 1978), which is influenced by: (a) hillslope morphology (i.e., slope, curvature, etc.) (Schmidt & Montgomery, 1995); (b) lithological characteristics, including the depth and bio-physiochemical properties of soil and underlying bedrock characteristics, including type, fracture density, and composition (Clarke & Burbank, 2011; Dixon et al., 2009; Phillips et al., 2005); (c) associated surface and subsurface hydrology; and (d) triggering mechanisms, such as precipitation, earthquakes, and anthropogenic activities (Lehmann et al., 2013; Varnes, 1978).

The impact of mass wasting on the weathering of sediment delivered to streams in high-relief and high-precipitation landscapes is not well known and may provide important evidence of historical weathering trends or could predict trends likely to occur with future mass wasting (Bluth & Kump, 1994; Joo et al., 2018). Mass wasting introduces a range of sediment grain sizes to fluvial systems (Larsen & Torres-Sánchez, 1998), which may also depend on several additional factors, including (a) bedrock lithology (Roda-Boluda et al., 2018), (b) rates of chemical weathering, particularly in tropical regions where more chemical weathering leads to finer grain sizes (Fernandes et al., 2016), and (c) transport mechanisms. In this study, underlying bedrock lithology and chemical weathering processes are held constant allowing us to further investigate the transport mechanisms. For example, sediment supplied from gradual erosion of soil via overland flow tends to be finer grained and more homogeneous (i.e., well-sorted) (Attal et al., 2015), while sediment supplied via landslides tends to be coarser and poorly sorted and can result in coarsening downstream compared to the general trend of distal fining expected in a typical fluvial system (Attal et al., 2015; Roda-Boluda et al., 2018; Struck et al., 2015). In addition, steep slopes in humid climates with abundant precipitation are more susceptible to mass wasting versus steep slopes in arid climates (Gariano & Guzzetti, 2016; Shiels & Walker, 2013).

Due to stochastic events, such as mass wasting, fluvial sediment properties can vary widely across both space and time. Anomalously low chemical index of alteration (CIA) values observed in fluvial sediments collected from the granitic watershed study area in Puerto Rico in 2014 were previously attributed to the significant influence of mass wasting that tapped less-weathered regolith (Joo et al., 2018). Joo et al. (2018) posited that future climate warming and attendant increased precipitation might further stimulate the delivery of hillslope material to streams, resulting in lower values of weathering indices in fluvial sediment. Hurricane Maria, which passed over Puerto Rico on 20 September 2017, resulted in >500 mm of rainfall within 48 hr (Silva-Tulla et al., 2020) and triggered widespread mass wasting in the study area (Bessette-Kirton et al., 2019; Keellings & Hernández Ayala, 2019; Ramos-Scharrón & Arima, 2019). This natural disaster caused enormous loss of life, health, and property (Bessette-Kirton et al., 2019; Keellings & Hernández Ayala, 2019; Lepore et al., 2012), but also created a natural experiment to directly observe the immediate impact of hurricane-induced mass wasting on fluvial sediments.

Joo et al. (2018) predicted that mass-wasting events supply the fluvial system with larger grains that are less weathered and derived from bedrock, regolith, or saprolite rather than soils. Additionally, they predicted that mass wasting would deliver not only larger grain sizes than systems without mass-wasting events, but also a wider range of grain sizes, and less weathered grains in the case of deep-seated landslides (Attal et al., 2015; Hubert & Filipov, 1989). However, the potential impact of transient hillslope responses to intense but short-duration precipitation events on fluvial sediments remains poorly constrained. In this study, we hypothesized that hurricane-induced landslides would sample deeper bedrock (Joo et al., 2018). To test this hypothesis, we investigated the short-term impact of a significant storm event—Hurricane Maria, and the resultant landslides on fluvial

sediment properties by comparing grainsize, mineralogy, and bulk chemistry of the fine-grained sediments within the system pre- and post-hurricane. This study aims to further our understanding of the interactions between chemical and physical weathering processes and investigate the application of chemical weathering indices as a proxy for climate signals in fluvial systems.

## 2. Background

### 2.1. Geology

The regional tectonic system of Puerto Rico is characterized by left-lateral slip deformation along the Puerto Rico Trench, resulting in the moderate earthquake activity and uplift rates of 1 mm/yr (Mann et al., 2005; Masson & Scanlo, 1991). The specific study region is a part of the Cordillera Central Mountain range in southeastern Puerto Rico, which is characterized by Jurassic to Eocene igneous bedrock with a number of normal faults (Monroe, 1980). Major drainages in the study area include the Rio Guayabo and Rio Guayanés, which also follow normal faults. The Rio Guayanés watershed is ~23 $km^2$ with a minimum elevation of 21 m and a maximum elevation of 539 m above sea level. The Rio Guayabo watershed is ~8.5 $km^2$ with a minimum elevation of 23 m and a maximum elevation of 497 m above sea level. Both fluvial systems are underlain by the Late Cretaceous San Lorenzo granodiorite (Rogers et al., 1979). In general, the granodiorite is overlain by ~2- to 8-m-thick saprolite and ~0.5- to 1-m-thick soil (Fletcher et al., 2006; Murphy et al., 2012).

### 2.2. Climate and Land Usage

A tropical wet climate prevails with an average annual temperature of ~25°C, an average annual rainfall of ~768 mm, and approximately one hurricane every 2 years (Larsen, 2000; Lepore et al., 2012). Subtropical wet forests and sparsely populated rural areas prevail now after agricultural land use declined by 95% from 1951 to 2000 (Birdsey & Weaver, 1982; Martinuzzi et al., 2007). During the sixteenth century, European settlers began massive deforestation to support agriculture, resulting in the destruction of the majority of mature forests by the nineteenth century (Birdsey & Weaver, 1982). Until the 1940s, sugarcane fueled the economy, driving near-total deforestation, with regional forest returning only since the 1950s as a result of the abandonment of small farms (Birdsey & Weaver, 1982). More recent anthropogenic activity in the form of road construction increases modern deforestation and destabilizes slopes; the highest density of landslides occur within close proximity to roads (Larsen & Parks, 1997; Tanyaş et al., 2022).

### 2.3. Mass Wasting

Landslides occur in mountainous terrains of Puerto Rico and cause loss of life and property (Bessette-Kirton et al., 2019; Keellings & Hernández Ayala, 2019; Lepore et al., 2012). Lepore et al. (2012) conducted a landslide susceptibility assessment of various areas in Puerto Rico and projected varying susceptibilities attributable in part to the underlying bedrock lithology (Bessette-Kirton et al., 2019; Hughes & Schulz, 2020). The severe deforestation and road density along with steep slopes and frequent high precipitation were observed in Puerto Rico alone or in conjunction with seismic activity and chemical weathering results in higher rates of erosion and mass wasting than in drier, less mountainous, or more forested terrains (Birdsey & Weaver, 1982; Hovius et al., 2011; Hughes & Schulz, 2020; Larsen & Parks, 1997; Wang et al., 2017).

### 2.4. Chemical Weathering Indices

Chemical weathering tends to be most intense in densely vegetated, tropical mountainous environments where surface and subsurface hydrologic fluxes are high (Oliva et al., 2003). The CIA is an indicator of the chemical weathering of feldspars to clays (Goldberg & Humayun, 2010). The CIA values of fluvial muds (<63 μm) have been quantified for some tropical and subtropical areas and are commonly used as a proxy for paleoclimate interpretations (Nesbitt & Young, 1982). The weathering of feldspars results in the removal of mobile cations, such as calcium, potassium, and sodium, which leads to an increase in the proportion of $Al_2O_3$ in the fluvial mud (Aristizábal et al., 2005; Nesbitt & Young, 1982). High CIA values (>90) are indicative of extensively weathered soil depleted in calcium and sodium and enriched in aluminum and values ≤50 are typical for unweathered

bedrock (Nesbitt & Young, 1982). CIA values are calculated using the following equation developed by Nesbitt and Young (1982), where CaO* is silicate-bound.

$$\mathrm{CIA} = \left[\frac{\mathrm{Al_2O_3}}{(\mathrm{Al_2O_3} + \mathrm{CaO^*} + \mathrm{Na_2O} + \mathrm{K_2O})}\right] \times 100 \quad (1)$$

The CIA values observed in fluvial mud samples collected from the study area in 2014 were abnormally low (58–69) compared to expected values (>90), considering that Puerto Rico exhibits very high weathering rates and a tropical-subtropical climate (Joo et al., 2018; White & Blum, 1995; White et al., 1998). Joo et al. (2018) noted that concentrations of CaO*, $Na_2O$, MgO, and $Fe_2O_3$ in the mud decreased distally, while $K_2O$ increased distally, suggesting that the degree of chemical weathering observed in the sediments increases downstream, perhaps due to preferential transport of clays.

Ohta and Arai (2007) developed an alternative approach to determine both primary source lithology and weathering intensity (Ohta & Arai, 2007). This approach uses wt% $SiO_2$, $TiO_2$, $Al_2O_3$, $Fe_2O_3$, MgO, CaO, $Na_2O$, and $K_2O$ in a multicomponent linear regression analysis to determine mafic (M) and felsic (F) portions of parent lithology and the degree of weathering (W) of mafic and felsic portions, independent of the parent rock. Ternary plots of MFW have been used to display the multiple components, assuming that normally distributed geochemical variability is typically found in fresh mafic, fresh felsic, and weathered rock (Ohta & Arai, 2007). The combined utilization of different weathering indices based on the major elemental components of the lithology can help illustrate the extent of alteration based on the degree of elemental loss (Babechuk et al., 2014).

## 3. Methods

### 3.1. Landslide Mapping

We used aerial images archived in Google Earth and 1 m lidar topographic data (USGS National Map, 2020) to map post-Hurricane Maria landslides within the entire polygon source area including runout (24 September 2017 to 9 June 2018) and 10 m USGS National Elevation Datasets to map hillslope geometries and drainage networks. Landslides were mapped only within a 350 m buffer of the Rio Guayanés and Rio Guayabo rivers based on our field observation that much of the sediments delivered to these streams appear to originate from landslides in adjacent hillslopes. The locations and characteristics of some of the landslides mapped from Google Earth and lidar shaded relief images were verified in the field and fall within the high to very high landslide susceptibility areas denoted by Bessette-Kirton et al. (2019). Landslide area was calculated in ArcGIS® and the volume of each landslide was modeled using an area ($A$) and volume ($V$) relationship ($V = 0.0254 \times A^{1.45}$) proposed by Regmi et al. (2014) for shallow landslides of the North Fork Gunnison River catchment of western Colorado. We apply this equation because of the similarity in geomorphic and lithological environments of this study with those of the North Fork Gunnison River catchment. In addition, the equation does not differ significantly from other area-volume relationships proposed for shallow landslides in various parts of the world (equations are listed in Regmi et al. (2014) and Tron et al. (2014)). However, a portion of the landslides mapped in this study are shallower than those documented in Regmi et al. (2014), suggesting the modeled volume and depths of some of the landslides in the Puerto Rico study may be slightly overestimated. The size (area, volume, and depth), frequency, and spatial density (Guzzetti et al., 2008) of observed landslides were then evaluated to explore if any relationship exists between spatial density and measured physiochemical characteristics of fluvial sediment.

### 3.2. Sediment and Water Sampling

Saprolite, fluvial sediment, and stream water samples were collected from the Rio Guayanés and Rio Guayabo in June 2018, 9 months post-Hurricane Maria, using GPS locations to ensure similar localities (<100 m away from 2014 sample locations) and sampling methods compared to Joo et al. (2018). Saprolite samples were obtained from roadcut slopes (Figure 1). The top 2–5 cm of fine-grained sediment samples were collected from the slack water areas of fluvial bars using a hand trowel at intervals ranging from ~1 to 5 km between sampling locations, beginning at the upland source of the stream and continuing ~21 km in a total distance downstream (Figure 1). Sampling locations were determined based on stream morphology and accessibility. Water samples were also collected from each of these locations. Sediment and water samples were frozen upon returning to the lab and prior to analyses.

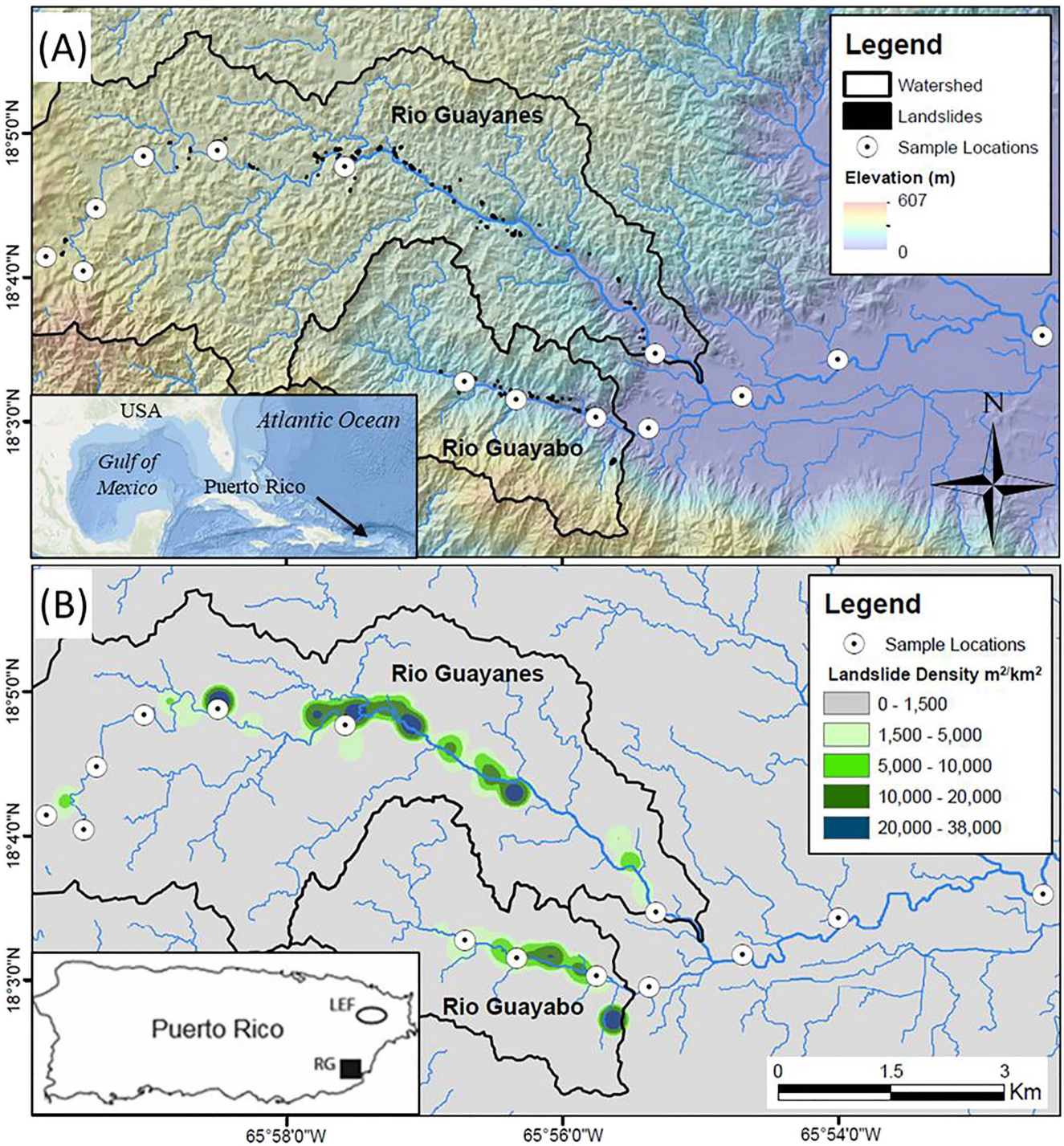


**Figure 1.** (a) Relief map of the Rio Guayanés located to the north and the Rio Guayabo in the south of the study region. Watersheds for the respective fluvial systems are outlined in black with sampling sites labeled as white circles and landslides indicated in black. (b) Inset map with the study region highlighted by black box (RG, LEF = Luquillo Long-Term Ecological Research area). Spatial density map for the study region was created using kernel density estimation of each of the mapped landslides within a 1 $km^2$ circular neighborhood. The large gap between sampling locations along the Rio Guayanés reflects the inability to access the sites as a direct result of hurricane damages.

### 3.3. Grain Size, Mineralogy, and Surface Area

All samples were wet sieved to obtain size fractions of gravel (>2 mm), sand (63 μm–2 mm), and mud (<63 μm) and then, the mud was treated with buffered acetic acid and hydrogen peroxide to remove carbonates (rare) and

**Table 1**
*Landslide Area, Volume[a], and Depth[a]*

| | | |
|---|---|---|
| Number of Landslides | | 116 |
| Area ($m^2$) | Minimum | 11 |
| | Mean (arith.) | 238 |
| | Maximum | 2,230 |
| Volume ($m^3$) | Minimum | 1 |
| | Mean (arith.) | 110 |
| | Maximum | 1,819 |
| Depth (m) | Minimum | 0 |
| | Mean (arith.) | 0 |
| | Maximum | 1 |

*Note*. The average area (~238 $m^2$) and volume (110 $m^3$) may indicate that the average depth of the landslides is very shallow (~0.25 m). Full data set in Supporting Information S1.

[a]Landslide volume was computed using the area-volume relationship proposed for western Colorado by Regmi et al. (2014) and the depth was computed as a ratio of volume and area.

organic matter (abundant), respectively. The remaining treated mud samples were freeze-dried prior to the specific surface area (SSA) analysis using the six-point BET nitrogen adsorption isotherm (Brunauer et al., 1938). The mud samples were passed through a 0.4 mm sieve to separate any clumps to prepare the sample for a random mounting (Harris & White, 2008) on a glass slide for powder X-ray diffraction (XRD) analysis using the Rigaku Ultima IV diffractometer using Cu-K-alpha radiation at 40 kV and 44 mA. We used the Bragg-Brentano method with a range of 2°–70° $2\theta$ at 0.02° step size. Resulting diffraction patterns were analyzed with MDI JADE Pro software and the ICDD PDF-4+ database by whole pattern fitting for bulk mineral identification.

### 3.4. Bulk Geochemical Analysis and Chemical Weathering Indices

A split (~3 to 3.5 g) of the processed mud was sent to ALS Labs, where the solid samples were dissolved in strong acid and analyzed using inductively coupled plasma (ICP)-atomic emission spectrometry. In a few cases, the sample volumes were too small for analysis, so we added a known amount of corundum standard and later corrected for the added $Al_2O_3$ in the results.

The CIA values of the fluvial sediment mud fraction were then calculated using Equation 1 and the resulting data plotted on a ternary diagram of CaO + $Na_2O$, $K_2O$, and $Al_2O_3$ with more weathered samples plotting toward the $Al_2O_3$ vertex. Additionally, following Ohta and Arai (2007), an alternative chemical weathering index was also computed based on the bulk chemistry data that can be used to characterize a mafic (M) and felsic (F) portion of rock source and the degree of weathering (W) (Equation S1, S2, S3 in Supporting Information S1) and plotted on an MFW ternary diagram with more weathered samples plotting toward the W vertex. We ran an ordinary two-way ANOVA and the Tukey's multiple comparison's test between the 2014 and 2018 CIA values for the Rio Guayanés and Rio Guayabo using GraphPad Prism software (v. 9.1.2). Family wise Alpha threshold was set to 0.05 and analyses were run within a 95% confidence interval.

### 3.5. Water Chemistry

Water samples collected in the field were filtered through a 0.22 µm filter using a Millipore vacuum system, treated with 1 M hydrochloric acid, and frozen. The samples were then sent to the Oklahoma State University Soil, Water and Forage Analytical Laboratory (http://soiltesting.okstate.edu/) where the samples were analyzed using ICP-optical emission spectrometry. The resulting data were used to plot aqueous cation concentration versus distance downstream to analyze chemical weathering solutes released from the sediment within the fluvial system.

## 4. Results

### 4.1. Mass Wasting

Both field and aerial photographic mapping suggest that Hurricane Maria triggered mostly shallow landslides. We identified 116 shallow landslides that occurred within ~350 m from Rio Guayanés and Rio Guayabo during the 9-month period following Hurricane Maria (Figure 1). The area of these landslides ranges from ~11 $m^2$ to ~2,230 $m^2$ with an average area of ~238 $m^2$ (Table 1, Figure 2a). Using the relationship in Regmi et al. (2014), the average volume is computed as ~110 $m^3$, and the average depth is computed as ~0.25 m with a standard deviation of 0.14 m (Table 1, Figure 2b). While the underlying bedrock and climate likely differ between Colorado and Puerto Rico, a spot analysis of scar depth and volume observed suggests that the model is a reasonable predictor.

The landslide size-frequency plot (Figure 2) suggests that most of the observed landslides are relatively small. The landslides occur across a wide range of gradients with the largest frequency occurring at ~24° to 26°, which also correlates with the most prevalent slopes in the area (Figure 2d). The average slopes of the entire landscape

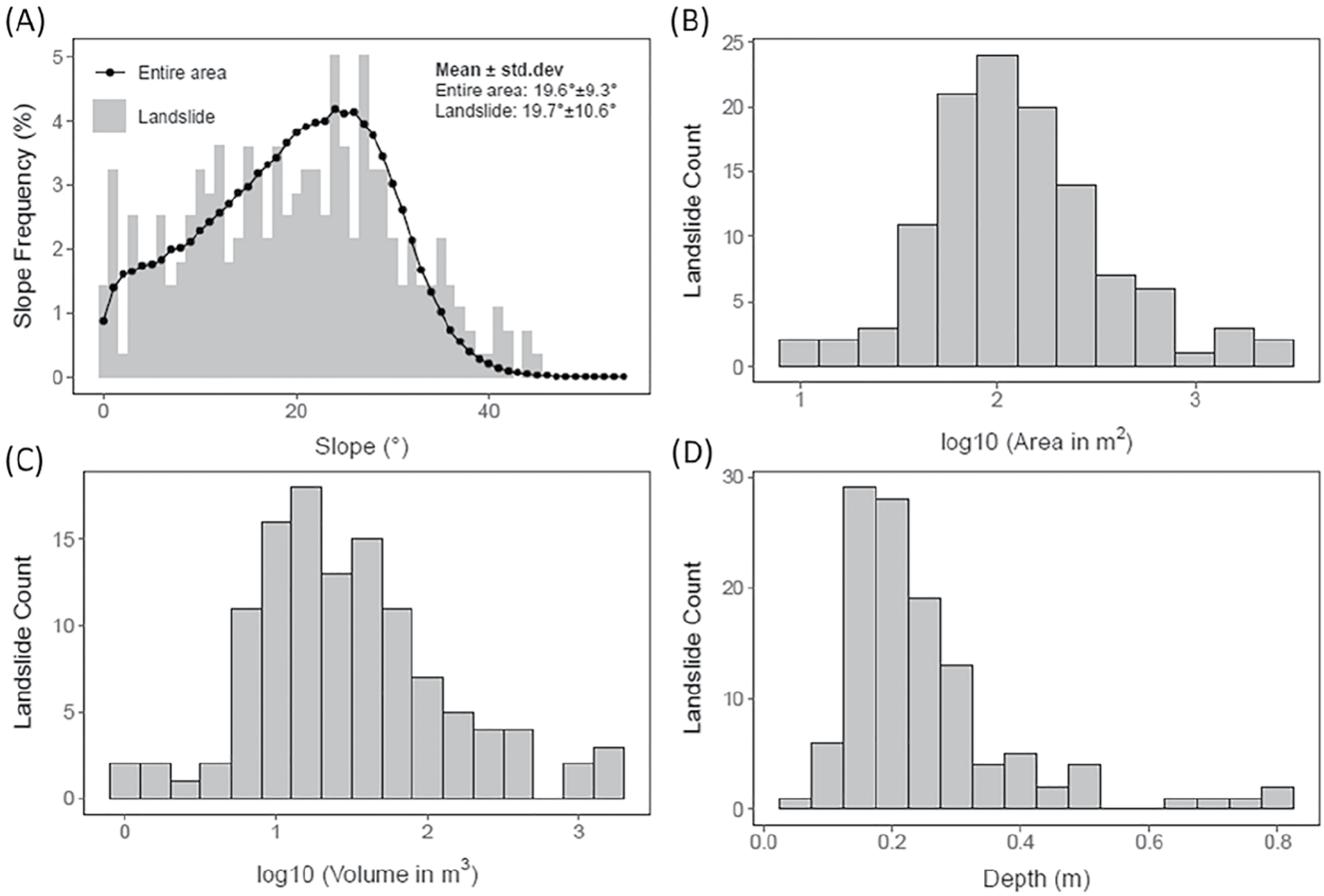


**Figure 2.** Observed hillslope characteristics including the distribution of slope gradients of landslides and entire watershed hillslopes (a), landslide area (b), modeled landslide volume (c), and modeled average landslide depth (d). Note that the landslide volume was computed using the landslide area—volume relationship proposed by Regmi et al. (2014), and the depth was computed as a ratio of volume and area. *Note*. Slope values were computed from DEM using a 30 × 30 m moving window, and their distribution within landslide polygons and the entire area were analyzed.

and areas containing landslides are 19.6° ± 9.3° and 19.7° ± 10.6°, respectively. Similarly, the landslide spatial density map developed using kernel density estimation and 1 km$^2$ circular neighborhood as a bandwidth shows the highest density of landslides between samples 5 and 7 along Rio Guayanés and between samples 3 and 4 of Rio Guayabo (Figure 1b).

### 4.2. Rio Guayanés Sediment

Overall, the sediment in the most proximal samples (closer to the head waters of the stream) is coarser and displays more variability in grainsize distributions observed between different samples in 2018 compared to 2014 (samples 1–3). For samples collected in both 2014 and 2018, the weight percent of sand is much higher (~75 wt%) than the weight percent of mud (<20 wt%) (Table S1 in Supporting Information S1). However, the proportions of the sand and mud fractions display a wider range of variability in the post-hurricane 2018 sample set. The weight percent of mud is generally 1–2 times higher in samples collected in 2018 from the proximal and distal portions of the stream compared to the weight percent of mud in 2014 samples from the same locations (Table S1 in Supporting Information S1). The weight percent of gravel observed in the samples collected from the mid-portion of the stream (samples 4–7) was slightly lower in 2018 than in 2014. The grain size of the sediments from the most distal samples (8–10) was also finer in 2018 with higher (5–25 wt%) gravel concentrations observed distally in 2014.

The 2018 and 2014 sample sets exhibit opposing trends in the weight percent of clay-sized grains along the stream course (Table S1 in Supporting Information S1): the 2018 samples show a higher proportion of clay-sized

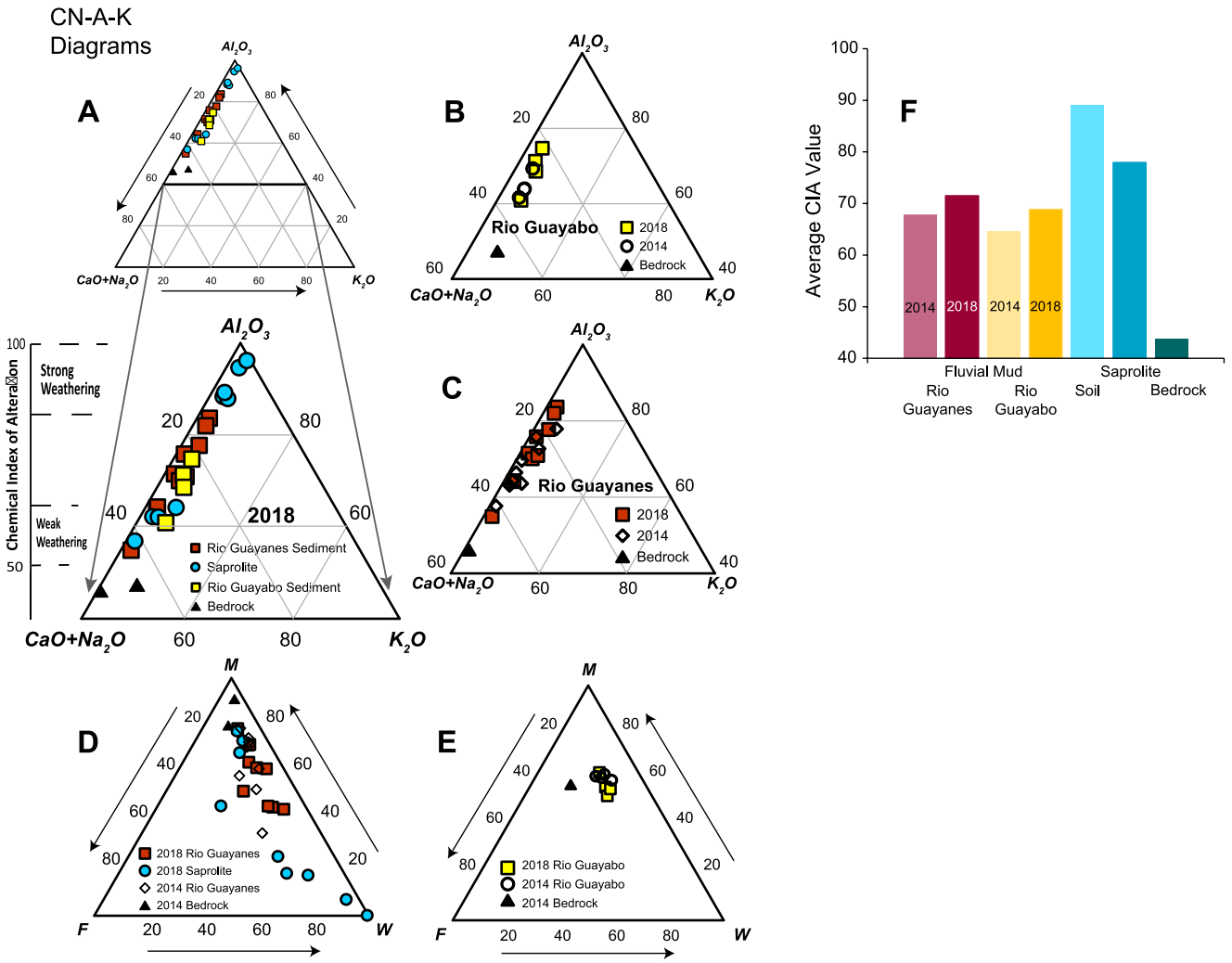


**Figure 3.** The chemical index of alteration (CIA) for all sample sets. (a) All of the samples collected in 2018 are shown on the left. Rio Guayanés sediment (red squares), saprolite samples (blue circles), Rio Guayabo sediment (yellow squares), and bedrock (black triangle). Panel (b) illustrates the CIA for the Rio Guayabo 2014 and 2018 samples, and panel (c) shows the Rio Guayanés 2014 and 2018 samples. The MFW plot of sediments sampled from hillslopes and bar deposits of Rio Guayanés River (d) and Rio Guayabo River (e) in 2014 (pre-hurricane) and 2018 (post-hurricane). *Note*. The 2018 fluvial sediments are more weathered than the 2014 bar sediments. (f) The average values of the CIA for all sediments, soil, saprolite, and bedrock samples.

material in more proximal samples (up to 17 wt%), whereas the 2014 samples display a higher (5 wt%) proportion of clay-sized grains in distal samples. Changes in the concentration of silt-sized grains are similar for both sampling years, but slightly higher (1–5 wt%) in 2018. The modal grain size within the mud fraction also shows opposing trends in the two sampling years, with the mud-sized modes increasing with distance downstream in 2018 and decreasing with distance downstream in 2014 (Table S1 in Supporting Information S1).

The mud size fraction collected in 2018 consists of mainly albite, quartz, amphibole, clay minerals, and mica (Table S2 in Supporting Information S1). No systematic change in mineralogy was observed from proximal to distal samples within the Rio Guayanés fluvial system in the 2018 samples, while the 2014 samples exhibited a general decrease in primary minerals (quartz, plagioclase, hornblende, and K-feldspar) in the distal samples (Joo et al., 2018).

The CIA values of the Rio Guayanés sediments on average indicate a higher degree of weathering in 2018, but also more variability than the values measured in the 2014 samples. The mean CIA value of the 2018 sediment is ~71, ranging from 54 to 83, while the mean value observed in the 2014 sediment is ~68, ranging from 57 to 78 (Figures 3 and 5). While the means and data distributions are visually different, a two-way ANOVA analysis of

the Rio Guayanés sediments showed no statistically significant difference ($p = 0.1354$) between the means of the 2014 and 2018 CIA values. Similar to the CIA values, the Rio Guayanés sediment MFW values also indicate that the 2018 sediment is more weathered when compared to 2014 samples (Figure 3; Joo et al., 2018). As the surface area of sediment increases, CIA values are also expected to increase since finer-grained sediment fractions have a higher surface area available for weathering and are also more likely to contain clay minerals (White et al., 1996). However, this relationship is only slightly observed in the 2018 Rio Guayanés sediment, while the expected trend is strongly observed in the 2014 Rio Guayanés sediment samples (Table S3 in Supporting Information S1).

### 4.3. Rio Guayabo Sediment

The surface area (13.74–15.97 $m^2/g$) in the 2018 Rio Guayabo sediment illustrates very little variability among the four sampling locations (Table S4 in Supporting Information S1). In the 2014 samples, there is a higher surface area in the proximal samples (24.64–32.05 $m^2/g$) and then the surface area decreases distally (15.41–15.74 $m^2/g$), reaching values similar to those observed throughout the 2018 samples (13.74–15.97 $m^2/g$).

The average CIA value of the 2018 Rio Guayabo sediment is 69 (ranging from 60 to 74), while the 2014 sediment average is lower at 64 (Figure 3). Both these values plot in the middle of the range of values observed in the Rio Guayanés sediment samples (Figure 3). Similar to the Rio Guayanés, while the means and data distributions are visually different, the two-way ANOVA analysis run for the Rio Guayabo sediments indicates no statistically significant difference ($p = 0.1354$) between the 2014 and 2018 mean CIA values. The Rio Guayabo MFW plot (Figures 3e and 3f) also indicates more weathered sediment in 2018 compared to 2014. Trends in CIA with the specific surface were very similar for both the 2018 and 2014 samples with CIA increasing as expected with the SSA (Table S5 in Supporting Information S1).

### 4.4. Saprolite

The grain-size distributions and the SSA of the mud-sized fractions observed in the saprolite samples collected within the watershed are highly variable. The mud-sized fractions of the saprolite samples consist mainly of clay minerals followed by plagioclase (Table S5 in Supporting Information S1). No systematic trends in mineralogy are observed within the saprolite data set. The saprolite samples have an average CIA value of 78, ranging from 56 to 96 (Figures 3 and 5), greater than the average values observed in the fluvial sediment samples from both the Rio Guayabo and Rio Guayanés (Figure 3). As the surface area of the saprolite sediment increases, a subsequent increase in the CIA value is also expected; this correlation is strongly observed within the saprolite samples (Table S5 in Supporting Information S1). The saprolite sediment MFW plot (Figures 3e and 3f) also indicates that the saprolite samples are significantly more weathered than the fluvial sediments.

### 4.5. Water Chemistry

The 2018 stream water samples had much higher concentrations of $Na^+$, $Ca^{2+}$, and $Mg^{2+}$ and a lower overall concentration in $K^+$ compared to the stream water in 2014 (Figure 4). In 2018, the $Na^+$, $Ca^{2+}$, and $Mg^{2+}$ concentrations generally decreased from proximal to distal until approximately 12 km, where an increase and then a subsequent decrease occurred (Figure 4). In the 2014 stream water samples, $Ca^{2+}$ and $Mg^{2+}$ have very similar concentrations and follow similar trends, while $Na^+$ was consistently enriched relative to the other solutes in 2018. $K^+$ concentrations increased from proximal to distal across the full distance sampled in 2018 (Figure 4).

## 5. Discussion

As expected, landslides were more common in the months following Hurricane Maria. Our data indicate 116 landslides occurred within the 9 months following Hurricane Maria. This is significantly higher than the background rate of six landslides per square kilometer in Puerto Rico (Larsen & Parks, 1997). The prevalence of landslides during this time likely reflects the heavy storm precipitation in addition to continued anthropogenic forcings, such as deforestation (Larsen & Parks, 1997; Murphy et al., 2012; Silva-Tulla et al., 2020). Additionally,

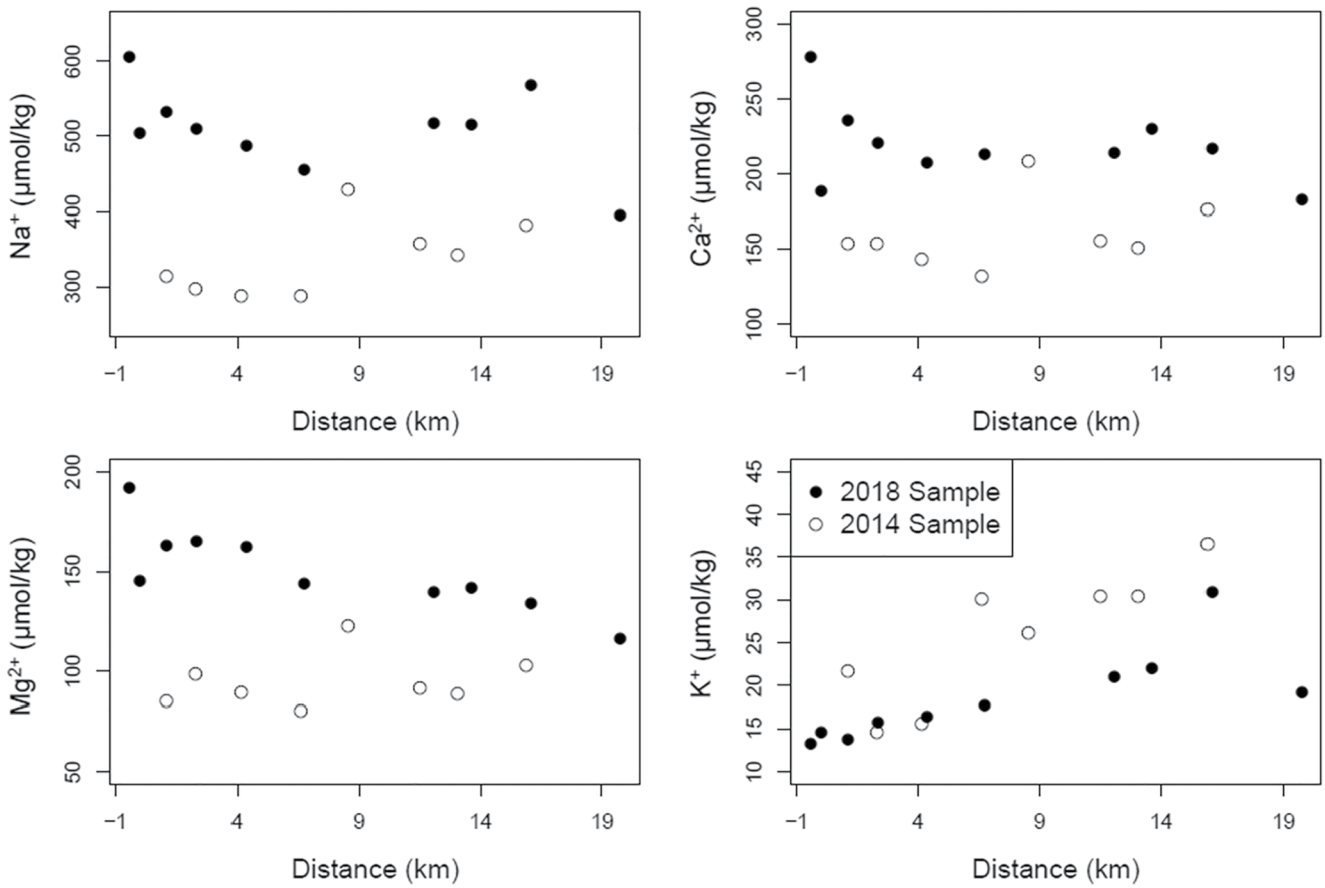


**Figure 4.** Rio Guayanés stream water chemistry cation concentrations. $Na^+$, $Ca^{2+}$, and $Mg^{2+}$ show a general decrease in concentration until approximately 12 km, and $K^+$ shows a general increase distally in 2018. $Mg^{2+}$ and $Ca^{2+}$ show very similar trends to one another, while $Na^+$ is enriched compared to $Mg^{2+}$ and $Ca^{2+}$ but also shows a similar trend. The −1 km indicates the distance above the confluence point of two smaller tributary streams that join to form the Rio Guayanés.

SSURGO soil texture data (U.S. Department of Agriculture and Soil conservation Service, 1977) show that predominant hillslopes are covered by weathered bedrock (mostly granodiorite) and silty clay soil, which contain organic materials. These characteristics of soil can facilitate rapid increases in pore-water pressure during a rainstorm event (C. Lepore et al., 2013) and predispose hillslopes to landslides. We initially hypothesized that hurricane-induced landslides would sample the deeper bedrock (Joo et al., 2018). However, our results indicate that the Hurricane Maria-induced landslides are dominated by shallow and small-sized landslides that moved mostly shallow slope materials, including weathered topsoil and saprolite, and only a small amount of less-weathered bedrock (Table S6 in Supporting Information S1) despite the precipitation of 0.5 m in 4 days. This model is well supported by all our results, including landslide mapping, similar observations made in Utuado, Puerto Rico (Bessette-Kirton et al., 2020), as well as the weathering index values and MFW plots for the post-hurricane fluvial samples, which were higher than those observed in pre-hurricane samples (Figure 3). However, some of the larger landslides that occurred in steeper slopes could have transported deeper soil and less-weathered bedrock, but the volume of the transported materials was likely small compared to the total volume transported by all landslides (Figure 2). Even larger or more sustained precipitation events may be more likely to produce deeper landslides.

We also expected the fluvial sediment grain size would increase post-Hurricane Maria due to the delivery of less-weathered sediments to the stream via landslides (Abbott et al., 2018; East et al., 2018). Instead, most of the samples from Rio Guayanés show decreased weight percent of gravel and increased weight percent of sand, mud, and silt size fractions in 2018 versus in 2014 (Figure S1 in Supporting Information S1). However, the pattern is more complicated if we consider the particle size modes (Struck et al., 2015) of the mud fraction, which indicates that coarser muds were delivered to the fluvial system upstream (sample locations 1–4), finer mid-stream (sample

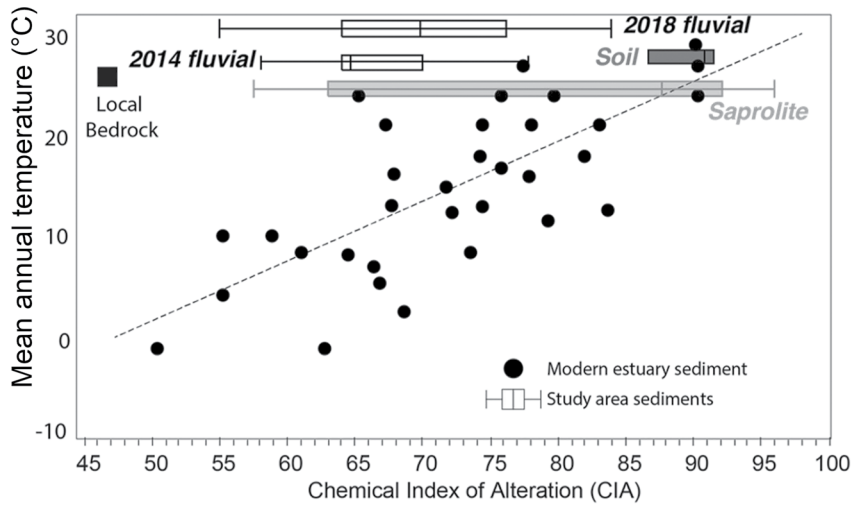


**Figure 5.** Chemical index of alteration values obtained from fluvial sediments (white boxes), soils (dark gray box), and saprolite (light gray box) collected in 2014 and 2018 (white boxes) do not fit the expected linear relationship between fine-grained sediments and mean annual temperatures reported in the literature. Only the soil values from the study area fall were expected on the trend line. The plot is modeled after and expanded from previous data reported in Joo et al. (2018).

locations 5–6), and coarser downstream (sample locations 7–10) (Figure 1). Overall, relatively coarser mud was delivered to the Rio Guayanés fluvial system in 2018 despite the overall finer grain size trend observed in the bulk sediment.

If landslides are the dominant source of sediment to the streams, we would not expect to see a trend in mineralogy as we moved downstream, but instead we would expect to see constant or variable mineralogy related to distance. Indeed, the mineralogy results from the XRD data indicate no systematic trend in mineralogy within the mud-sized fraction from proximal to distal regions of the rivers (Table S2 in Supporting Information S1). Since we observed no systematic trend downstream in both particle mode and mineralogy, this indicates little sorting within the fluvial system, nor is there a significant change in the sediment source from proximal to distal stretches of the stream.

Results from the aqueous cation concentrations in the stream were similar to the results obtained by Joo et al. (2018), in which the $Na^+$, $Ca^{2+}$, and $Mg^{2+}$ generally decreased distally, while the $K^+$ increased (Figure 4). However, the overall concentration of the solutes in 2018 was greater than in 2014 for every cation with the exception of $K^+$ (Figure 4). This suggests that landslides impact fluvial systems by delivering both solutes and sediments to streams. Increased cation concentrations may lead to eventual carbonate precipitation downstream following a mass-wasting event, resulting in a net carbon sink (Joo et al., 2018).

The anomalously low CIA values observed in the fluvial sediments collected before Hurricane Maria (Figures 3 and 5; Joo et al., 2018) were previously interpreted as deriving from deep-seated landslides that delivered partially weathered regolith to the fluvial systems. These deeper seated landslides could be a result of tectonics and therefore earthquakes (Bessette-Kirton et al., 2019; Masson & Scanlo, 1991; Reid & Taber, 1919) and/or anthropogenic forcing, such as the construction of roads in the hillsides (Larsen & Parks, 1997; Murphy et al., 2012). In addition, there may also be a time-dependent sediment accumulation/depletion effect. For example, the fluvial sediments collected in 2014 may be the accumulated results of deposits from large landslides over a longer period of time, whereas this study reports the response of a rapid flux of sediment from very shallow landslides triggered by a short duration but intense rainfall. The last severe weather event in Puerto Rico prior to 2014 was Hurricane Irene of 2011. It is possible that streams may have removed much of the sediments delivered by Irene-induced shallow landslides by 2014, and the 2014 observations of Joo et al. (2018) indicate time-averaged sediment properties. While the overall transport mechanism is essentially the same, variations in the initial cause of the mass wasting and the duration of sediment transport between the events likely differ. In either case, the change in weathering index values observed in the sediment record is not indicative of long-term climate (Figure 5) but instead a reflection of the stochastic nature of mass wasting.

## 6. Conclusions and Implications

While the initial disturbance of mass-wasting events can trigger carbon release to the atmosphere through the perturbation of the short-term carbon cycle (e.g., destruction of vegetation), a longer-term result has increased silicate weathering, leading to a drawdown of atmospheric carbon (Fisk et al., 2013; Hall et al., 2020). The exposure of fresh bedrock through mechanical weathering due to landslides accentuates chemical weathering as water and oxygen interact with fresh bedrock (Oliva et al., 2003). Fresh surfaces lack weathered rindlets (Turner et al., 2003), soils, or clay, thus enhancing susceptibility to chemical weathering (White et al., 1998). Likewise, the sediment released by landslides can remain stored on hillslopes or delivered to fluvial systems (Clark et al., 2016; Hilton et al., 2011). Deposition of the material on hillslopes can result in longer-term carbon sequestration due to chemical weathering of the transported material (Clark et al., 2016; Fisk et al., 2013; Hall et al., 2020; Hilton et al., 2011; Ramos Scharrón et al., 2012). Sediments entering fluvial systems tend to have a more variable and unconstrained outcome in regard to carbon sequestration (Clark et al., 2016; Ramos Scharrón et al., 2012) but precipitation and deposition of carbonates that consume cations released via chemical weathering result in a long-term net carbon sink. The landslide scarps sequester carbon over periods of tens to hundreds of years as forest recovery sequesters more carbon in both plants and soils compared to mature forests (Fisk et al., 2013; Hall et al., 2020; Hilton et al., 2011). Our data also demonstrate that even relatively small landslides can increase cation fluxes into stream systems, which deliver cations to the ocean where carbonate minerals likely precipitate, thus further accentuating the carbon sink. Therefore, the magnitude of a storm and associated rainfall accumulation amounts coupled with a variety of variables, such as lithology, anthropogenic disturbances, and degree of hillslope, can significantly affect carbon sequestration.

In addition, this study also provides high-resolution data that show how the grain size and chemistry of fluvial sediments vary over time in systems heavily influenced by mass wasting across the sediment transport route. Our results show that hillslope dynamics closely influence fluvial sediment properties and may provide an avenue for interpreting the relative size of landslides based on trends in fluvial sediment observed in close temporal proximity of the triggering event.

Significant differences in the weathering indices observed that pre- and post-Hurricane Maria do not reflect the degree of climate change over 4 years, but rather indicative of numerous small landslide events that released large volumes of pre-weathered soil and saprolite materials into the fluvial system. Lower weathering index values observed before the hurricane are likely due to deep-seated landslides caused by tectonics, longer-term groundwater fluctuations, or road building that sampled deeper, less weathered materials, including bedrock and regolith. Therefore, this subtle change in the transport mechanism can result in rather large differences in the weathering values recorded by the fluvial system.

## Data Availability Statement

The bulk chemistry, mineralogy, and grainsize data used in our study "Effects of mass wasting on the physiochemical properties of fluvial sediments in Puerto Rico following Hurricane Maria" in the study are available at (Webb et al., 2022) Earthchem via doi: https://doi.org/10.26022/IEDA/112287, https://ecl.earthchem.org/view.php?id=2287 with open access to download the data set.

**Acknowledgments**
The authors appreciate helpful comments from three anonymous reviewers, Editor Amy East, and Associate Editor Craig Rasmussen, which improved the manuscript. Funding was provided by the National Science Foundation grant EAR-1543344. The authors thank the University of Oklahoma for funding publication costs.

## References

Abbott, S., Julian, J. P., Kamarinas, I., Meitzen, K. M., Fuller, I. C., McColl, S. T., & Dymond, J. R. (2018). State-shifting at the edge of resilience: River suspended sediment responses to land use change and extreme storms. *Geomorphology*, *305*, 49–60. https://doi.org/10.1016/j.geomorph.2017.09.004

Aristizábal, E., Roser, B., & Yokota, S. (2005). Tropical chemical weathering of hillslope deposits and bedrock source in the Aburrá Valley, northern Colombian Andes. *Engineering Geology*, *81*(4), 389–406. https://doi.org/10.1016/j.enggeo.2005.08.001

Attal, M., Mudd, S. M., Hurst, M. D., Weinman, B., Yoo, K., & Naylor, M. (2015). Impact of change in erosion rate and landscape steepness on hillslope and fluvial sediments grain size in the Feather River basin (Sierra Nevada, California). *Earth Surface Dynamics*, *3*(1), 201–222. https://doi.org/10.5194/esurf-3-201-2015

Babechuk, M. G., Widdowson, M., & Kamber, B. S. (2014). Quantifying chemical weathering intensity and trace element release from two contrasting basalt profiles, Deccan Traps, India. *Chemical Geology*, *363*, 56–75. https://doi.org/10.1016/j.chemgeo.2013.10.027

Berner, R. A. (1995). Chemical weathering and its effect on atmospheric $CO_2$ and climate. In A. F. White & S. L. Brantley (Eds.) *Chemical weathering rates of silicate minerals* (Vol. 31, pp. 565–583).

Bessette-Kirton, E. K., Cerovski-Darriau, C., Schulz, W. H., Coe, J. A., Kean, J. W., Godt, J. W., et al. (2019). Landslides triggered by Hurricane Maria: Assessment of an extreme event in Puerto Rico. *Geological Society of America Today*, *29*(6). https://doi.org/10.1130/GSATG383A.1

Bessette-Kirton, E. K., Coe, J. A., Schulz, W. H., Cerovski-Darriau, C., & Einbund, M. M. (2020). Mobility characteristics of debris slides and flows triggered by Hurricane Maria in Puerto Rico. *Landslides*, *17*(12), 2795–2809. https://doi.org/10.1007/s10346-020-01445-z

Birdsey, R. A., & Weaver, P. L. (1982). The forest resources of Puerto Rico. *Resource Bulletin SO 85*, *85*, 59. https://doi.org/10.2737/so-rb-85

Bluth, G. J. S., & Kump, L. R. (1994). Lithologic and climatologic controls of river chemistry. *Geochimica et Cosmochimica Acta*, *58*(10), 2341–2359. https://doi.org/10.1016/0016-7037(94)90015-9

Brunauer, S., Emmett, P. H., & Teller, E. (1938). *Adsorption of gases in multimolecular layers*. Retrieved from https://pubs.acs.org/sharingguidelines

Clark, K. E., West, A. J., Hilton, R. G., Asner, G. P., Quesada, C. A., Silman, M. R., et al. (2016). Storm-triggered landslides in the Peruvian Andes and implications for topography, carbon cycles, and biodiversity. *Earth Surface Dynamics*, *4*(1), 47–70. https://doi.org/10.5194/esurf-4-47-2016

Clarke, B. A., & Burbank, D. W. (2011). Quantifying bedrock-fracture patterns within the shallow subsurface: Implications for rock mass strength, bedrock landslides, and erodibility. *Journal of Geophysical Research*, *116*(4), F04009. https://doi.org/10.1029/2011JF001987

Dixon, J. L., Heimsath, A. M., Kaste, J., & Amundson, R. (2009). Climate-driven processes of hillslope weathering. *Geology*, *37*(11), 975–978. https://doi.org/10.1130/G30045A.1

East, A. E., Stevens, A. W., Ritchie, A. C., Barnard, P. L., Campbell-Swarzenski, P., Collins, B. D., & Conaway, C. H. (2018). A regime shift in sediment export from a coastal watershed during a record wet winter, California: Implications for landscape response to hydroclimatic extremes. *Earth Surface Processes and Landforms*, *43*(12), 2562–2577. https://doi.org/10.1002/esp.4415

Emberson, R., Galy, A., & Hovius, N. (2018). Weathering of reactive mineral phases in landslides acts as a source of carbon dioxide in mountain belts. *Journal of Geophysical Research: Earth Surface*, *123*(10), 2695–2713. https://doi.org/10.1029/2018JF004672

Fernandes, A. M., da Conceição, F. T., Spatti Junior, E. P., de Souza Sardinha, D., & Mortatti, J. (2016). Chemical weathering rates and atmospheric/soil $CO_2$ consumption of igneous and metamorphic rocks under tropical climate in southeastern Brazil. *Chemical Geology*, *443*, 54–66. https://doi.org/10.1016/j.chemgeo.2016.09.008

Fisk, J. P., Hurtt, G. C., Chambers, J. Q., Zeng, H., Dolan, K. A., & Negrón-Juárez, R. I. (2013). The impacts of tropical cyclones on the net carbon balance of eastern US forests (1851–2000). *Environmental Research Letters*, *8*(4), 045017. https://doi.org/10.1088/1748-9326/8/4/045017

Fletcher, R. C., Buss, H. L., & Brantley, S. L. (2006). A spheroidal weathering model coupling porewater chemistry to soil thicknesses during steady-state denudation. *Earth and Planetary Science Letters*, *244*(1–2), 444–457. https://doi.org/10.1016/j.epsl.2006.01.055

Frith, N. V., Hilton, R. G., Howarth, J. D., Gröcke, D. R., Fitzsimons, S. J., Croissant, T., et al. (2018). Carbon export from mountain forests enhanced by earthquake-triggered landslides over millennia. *Nature Geoscience*, *11*(10), 772–776. https://doi.org/10.1038/s41561-018-0216-3

Gariano, S. L., & Guzzetti, F. (2016). Landslides in a changing climate. *Earth-Science Reviews*, *162*, 227–252. https://doi.org/10.1016/j.earscirev.2016.08.011

Goldberg, K., & Humayun, M. (2010). The applicability of the chemical index of alteration as a paleoclimatic indicator: An example from the Permian of the Paraná Basin, Brazil. *Palaeogeography, Palaeoclimatology, Palaeoecology*, *293*(1–2), 175–183. https://doi.org/10.1016/j.palaeo.2010.05.015

Guzzetti, F., Ardizzone, F., Cardinali, M., Galli, M., Reichenbach, P., & Rossi, M. (2008). Distribution of landslides in the Upper Tiber River basin, central Italy. *Geomorphology*, *96*(1–2), 105–122. https://doi.org/10.1016/j.geomorph.2007.07.015

Hall, J., Muscarella, R., Quebbeman, A., Arellano, G., Thompson, J., Zimmerman, J. K., & Uriarte, M. (2020). Hurricane-induced rainfall is a stronger predictor of tropical forest damage in Puerto Rico than maximum wind speeds. *Scientific Reports*, *10*(1), 1–10. https://doi.org/10.1038/s41598-020-61164-2

Harris, W., & G. N. White (2008). *X-ray diffraction techniques for soil mineral identification*. Methods of Soil Analysis Part 5-Mineralogical Methods, SSSA Book Series:5, 81–115.

Hilton, R. G., Meunier, P., Hovius, N., Bellingham, P. J., & Galy, A. (2011). Landslide impact on organic carbon cycling in a temperate montane forest. *Earth Surface Processes and Landforms*, *36*(12), 1670–1679. https://doi.org/10.1002/esp.2191

Hovius, N., Meunier, P., Lin, C. W., Chen, H., Chen, Y. G., Dadson, S., et al. (2011). Prolonged seismically induced erosion and the mass balance of a large earthquake. *Earth and Planetary Science Letters*, *304*(3–4), 347–355. https://doi.org/10.1016/j.epsl.2011.02.005

Hubert, J. F., & Filipov, A. J. (1989). Debris-flow deposits in alluvial fans on the west flank of the White Mountains, Owens Valley, California, USA. *Sedimentary Geology*, *61*(3–4), 177–205. https://doi.org/10.1016/0037-0738(89)90057-2

Hughes, K. S., & Schulz, W. (2020). *Map Depicting susceptibility to landslides triggered by intense rainfall, Puerto Rico*. Open-File Report, 67. https://doi.org/10.3133/ofr20201022

Joo, Y. J., Madden, M. E. E., & Soreghan, G. S. (2018). Anomalously low chemical weathering in fluvial sediment of a tropical watershed (Puerto Rico). *Geology*, *46*(8), 691–694. https://doi.org/10.1130/G40315.1

Keellings, D., & Hernández Ayala, J. J. (2019). Extreme rainfall associated with Hurricane Maria over Puerto Rico and its connections to climate variability and change. *Geophysical Research Letters*, *46*(5), 2964–2973. https://doi.org/10.1029/2019GL082077

Larsen, M. C. (2000). Analysis of 20th century rainfall and streamflow to characterize drought and water resources in Puerto Rico. *Physical Geography*, *21*(6), 494–521. https://doi.org/10.1080/02723646.2000.10642723

Larsen, M. C., & Parks, J. E. (1997). How wide is a road? The association of roads and mass-wasting in a forested montane environment. *Earth Surface Processes and Landforms*, *22*(9), 835–848. https://doi.org/10.1002/(SICI)1096-9837(199709)22:9<835::AID-ESP782>3.0.CO;2-C

Larsen, M. C., & Torres-Sánchez, A. J. (1998). The frequency and distribution of recent landslides in three montane tropical regions of Puerto Rico. *Geomorphology*, *24*(4), 309–331. https://doi.org/10.1016/S0169-555X(98)00023-3

Lehmann, P., Gambazzi, F., Suski, B., Baron, L., Askarinejad, A., Sarah, M., et al. (2013). Evolution of soil wetting patterns preceding a hydrologically induced landslide inferred from electrical resistivity survey and point measurements of volumetric water content and pore water pressure. *Water Resources Research*, *49*(12), 7992–8004. https://doi.org/10.1002/2013WR014560

Lepore, C., Arnone, E., Noto, L. V., Sivandran, G., & Bras, R. L. (2013). Physically based modeling of rainfall-triggered landslides: A case study in the Luquillo forest, Puerto Rico. *Hydrology and Earth System Sciences*, *17*(9), 3371–3387. https://doi.org/10.5194/hess-17-3371-2013

Lepore, C., Kamal, S. A., Shanahan, P., & Bras, R. L. (2012). Rainfall-induced landslide susceptibility zonation of Puerto Rico. *Environmental Earth Sciences*, *66*(6), 1667–1681. https://doi.org/10.1007/s12665-011-0976-1

Mann, P., Prentice, C. S., Hippolyte, J. C., Grindlay, N. R., Abrams, L. J., & Laó-Dávila, D. (2005). Reconnaissance study of late quaternary faulting along cerro GoDen fault zone, western Puerto Rico. *Special Papers – Geological Society of America*, *385*, 115–137. https://doi.org/10.1130/0-8137-2385-X.115

Martinuzzi, S., Gould, W. A., & Ramos González, O. M. (2007). Land development, land use, and urban sprawl in Puerto Rico integrating remote sensing and population census data. *Landscape and Urban Planning*, *79*(3–4), 288–297. https://doi.org/10.1016/j.landurbplan.2006.02.014

Masson, D. G., & Scanlo, K. M. (1991). The neotectonic setting of Puerto Rico. *GSA Bulletin*, *103*(1), 144–154. https://doi.org/10.1130/0016-7606(1991)103<0144:tnsopr>2.3.co;2

Monroe, W. H. (1980). *Geology of the Middle Tertiary formations of Puerto Rico*. US Geological Survey, Professional Paper, 953.
Moore, O. W., Buss, H. L., & Dosseto, A. (2019). Incipient chemical weathering at bedrock fracture interfaces in a tropical critical zone system, Puerto Rico. *Geochimica et Cosmochimica Acta*, *252*, 61–87. https://doi.org/10.1016/j.gca.2019.02.028
Murphy, S. F., Stallard, R. F., Larsen, M. C., & Gould, W. A. (2012). Physiography, geology, and land cover of four watersheds in eastern Puerto Rico. *Water Quality and Landscape Processes of Four Watersheds in Eastern Puerto Rico*, 1–24.
Nesbitt, H. W., & Young, G. M. (1982). Early Proterozoic climates and plate motions inferred from major element chemistry of Intites. *Nature*, *299*(5885), 715–717. https://doi.org/10.1038/299715a0
Ohta, T., & Arai, H. (2007). Statistical empirical index of chemical weathering in igneous rocks: A new tool for evaluating the degree of weathering. *Chemical Geology*, *240*(3–4), 280–297. https://doi.org/10.1016/j.chemgeo.2007.02.017
Oliva, P., Viers, J., & Dupré, B. (2003). Chemical weathering in granitic environments. *Chemical Geology*, *202*(3–4), 225–256. https://doi.org/10.1016/j.chemgeo.2002.08.001
Phillips, J. D., Marion, D. A., Luckow, K., & Adams, K. R. (2005). Nonequilibrium regolith thickness in the Ouachita Mountains. *The Journal of Geology*, *113*(3), 325–340. https://doi.org/10.1086/428808
Ramos-Scharrón, C. E., & Arima, E. (2019). Hurricane María's precipitation signature in Puerto Rico: A conceivable presage of rains to come. *Scientific Reports*, *9*(1), 15612. https://doi.org/10.1038/s41598-019-52198-2
Ramos Scharrón, C. E., Castellanos, E. J., & Restrepo, C. (2012). The transfer of modern organic carbon by landslide activity in tropical montane ecosystems. *Journal of Geophysical Research*, *117*(3), 1–18. https://doi.org/10.1029/2011JG001838
Regmi, N. R., Giardino, J. R., & Vitek, J. D. (2014). Characteristics of landslides in western Colorado, USA. *Landslides*, *11*(4), 589–603. https://doi.org/10.1007/s10346-013-0412-6
Reid, H. F., & Taber, S. (1919). The Porto Rico Earthquakes of October–November, 1918. *Bulletin of the Seismological Society of America*, *9*(7), 95–127. https://doi.org/10.1785/BSSA0090040095
Roda-Boluda, D. C., D'Arcy, M., McDonald, J., & Whittaker, A. C. (2018). Lithological controls on hillslope sediment supply: Insights from landslide activity and grain size distributions. *Earth Surface Processes and Landforms*, *43*(5), 956–977. https://doi.org/10.1002/esp.4281
Rogers, C. L., Cram, C. M., Pease, M. H., and Tischler, M. S. (1979). *Geologic map of the Yabucoa and Punta Tuna quadrangles, Puerto Rico*. US Geological Survey Miscellaneous Investigations Series Map I-1086. Retrieved from https://ngmdb.usgs.gov/Prodesc/proddesc_8939.htm
Sassa, K., & Canuti, P. (2009). *Disaster risk reduction*. Springer Verlag.
Schmidt, K. M., & Montgomery, D. R. (1995). Limits to relief. *Science*, *270*(5236), 617–620. https://doi.org/10.1126/science.270.5236.617
Shiels, A. B., & Walker, L. A. (2013). Landslides cause spatial and temporal gradients at multiple scales in the Luquillo Mountains of Puerto Rico. *Ecological Bulletins*, *54*, 211–221. Retrieved from https://www.aphis.usda.gov/wildlife_damage/nwrc/publications/13pubs/shiels134.pdf
Silva-Tulla, F., Pando, M. A., Pradel, D., Park, Y., & Kayen, R. (2020). Geotechnical consequences and failures in Puerto Rico due to Hurricane Maria. *Geo-Congress*, *1*, 640–648.
Stark, C. P., & Hovius, N. (2001). The characterization of landslide size distributions. *Geophysical Research Letters*, *28*(6), 1091–1094. https://doi.org/10.1029/2000gl008527
Struck, M., Andermann, C., Hovius, N., Korup, O., Turowski, J. M., Bista, R., et al. (2015). Monsoonal hillslope processes determine grain size-specific suspended sediment fluxes in a trans-Himalayan river. *Geophysical Research Letters*, *42*(7), 2302–2308. https://doi.org/10.1002/2015GL063360
Tanyaş, H., Görüm, T., Kirschbaum, D., & Lombardo, L. (2022). Could road constructions be more hazardous than an earthquake in terms of mass movement? *Natural Hazards*, *112*(1), 0123456789. https://doi.org/10.1007/s11069-021-05199-2
Tron, S., Dani, A., Laio, F., Preti, F., & Ridolfi, L. (2014). Mean root depth estimation at landslide slopes. *Ecological Engineering*, *69*, 118–125. https://doi.org/10.1016/j.ecoleng.2014.03.019
Turner, B. F., Stallard, R. F., & Brantley, S. L. (2003). Investigation of in situ weathering of quartz diorite bedrock in the Rio Icacos basin, Luquillo Experimental Forest, Puerto Rico. *Chemical Geology*, *202*(3–4), 313–341. https://doi.org/10.1016/j.chemgeo.2003.05.001
U.S. Department of Agriculture and Soil Conservation Service. (1977). *Soil Survey of Humacao Area of Eastern Puerto Rico*. In U.S. Department of Agriculture, Soil Conservation Service (pp. 1–103).
USGS National Map. (2020). *USGS National Map*. Retrieved from https://viewer.nationalmap.gov/basic/
Varnes, D. (1978). Slope movement types and processes. *Special Report*, *176*, 11–33.
Wang, W., Godard, V., Liu-Zeng, J., Scherler, D., Xu, C., Zhang, J., et al. (2017). Perturbation of fluvial sediment fluxes following the 2008 Wenchuan earthquake. *Earth Surface Processes and Landforms*, *42*(15), 2611–2622. https://doi.org/10.1002/esp.4210
Webb, N. D. S., Regmi, N. R., Soreghan, G., Elwood Madden, A. S., Sylvester, J., Cartagena Colon, F., et al. (2022). Effects of mass wasting on fluvial sediments in Puerto Rico following Hurricane Maria, Version 1.0 [Data set]. Interdisciplinary Earth Data Alliance (IEDA). https://doi.org/10.26022/IEDA/112287
White, A. F., & Blum, A. E. (1995). Effects of climate on chemical, weathering in watersheds. *Pergamon Geochimica et Cosmochimica Acta*, *59*(9), 1729–1747. https://doi.org/10.1016/0016-7037(95)00078-e
White, A. F., Blum, A. E., Schulz, M. S., Bullen, T. D., Harden, J. W., & Peterson, M. L. (1996). Chemical weathering of a soil chronosequence on granite alluvium I. Reaction rates based on changes in soil mineralogy. *Geochimica et Cosmochimica Acta*, *60*(14), 2533–2550. https://doi.org/10.1016/0016-7037(96)00106-8
White, A. F., Blum, A. E., Schulz, M. S., Vivit, D. V., Stonestrom, D. A., Larsen, M., et al. (1998). Chemical weathering in a tropical watershed, Luquillo Mountains, Puerto Rico: I. Long-term versus short-term weathering fluxes. *Geochimica et Cosmochimica Acta*, *62*(2), 209–226. https://doi.org/10.1016/S0016-7037(97)00335-9
White, A. F., Bullen, T. D., Vivit, D. V., Schulz, M. S., & Clow, D. W. (1999). The role of disseminated calcite in the chemical weathering of granitoid rocks. *Geochimica et Cosmochimica Acta*, *63*(13–14), 1939–1953. https://doi.org/10.1016/S0016-7037(99)00082-4